

Fig. 5 Comparison of the effects of air and helium injection on aft-body drag coefficient for a 1 caliber 6° boat-tail.

that the velocity of the injected flow for the smallest orifice is becoming significant at the higher injection rates shown. This result is in agreement with earlier studies.⁴ Figure 2 clearly shows the significant decrease in drag resulting from small base blowing rates. For the largest injection orifice diameter, the base drag coefficient is almost halved at injection rates of $I=0.03$.

The effect of air injection on aft-body drag coefficient for three 6° boat-tail aft-bodies of lengths 1, $\frac{3}{4}$, and $\frac{1}{2}$ calibers, and a configuration without boat-tailing is shown in Fig. 3. For the latter configuration, the midpoints between the curves for $D=0.75$ in. and 0.50 in. of Fig. 2 were taken to conform with the orifice diameter of $D=0.625$ inches for all the boat-tail configurations.

The advantage of a long boat-tail is evident from the consistently lower drag coefficient obtained with each increase in length. Physically, this is explained by the fact that the pressure rises along the boat-tail length so that the longer the boat-tail, the higher the pressure at its trailing edge, which in turn, results in a higher base pressure and, therefore, lower drag. The rate of decrease in drag can be expected to drop off with much further increase in boat-tail length.²

The effect of boat-tail angle on aft-body drag coefficient for various rates of injection is shown in Fig. 4. Note that, without injection, boat-tails of 6°, 9°, and 12° result in about an equal reduction in aft-body drag. However, with base injection, minimum drag occurs for a boat-tail angle in the neighborhood of 6°.

The results for base injection of helium show similar qualitative trends to those for air, e.g., steady decrease in drag with increasing boat-tail length, minimum drag configuration with injection for a boat-tail angle in the neighborhood of 6°. However, quantitatively, with helium injection, the mass flow rates are considerably smaller than those for air for a given base pressure rise and the base pressure continues to rise well above the peaks obtained with air injection. Thus, lower drag values are obtained with helium.

Figure 5 gives a sample comparison of results for air and helium injection for a 6° boat-tail, 1 caliber long, clearly illustrating the lower injection rates and lower drag obtainable with a light gas. The helium results are expected to be somewhat closer than those of air to the high temperature,

low density products of combustion of fumers used in practical projectile applications.¹⁰

References

- ¹Murthy, S.N.B. and Osborn, J.R., "Base Flow Data With and Without Injection: Bibliography and Semi-Rational Correlations," Contract DAAD 05-72-C-0342, (BRL), School of Mechanical Engineering, Purdue University, May 1973.
- ²Sedney, R., "Review of Base Drag," Rept. 1337, Ballistic Research Laboratories, Aberdeen Proving Ground, Md., Oct 1966.
- ³Cortright, E.M., Jr. and Schroeder, A.H., "Preliminary Investigation of Effectiveness of Base Bleed in Reducing Drag of Blunt-Base Bodies in Supersonic Stream," NACA RM E51A26, March 1951.
- ⁴Bowman, J.E. and Clayden, W.A., "Base Pressure on a Boat-Tailed Afterbody at $M_\infty=2$ with Gas Ejection from Porous and Multi-Nozzle Bases," Memorandum 20/70, Royal Armament Research and Development Establishment, Fort Halstead, Kent, U.K., Aug. 1970.
- ⁵Bowman, J.E. and Clayden, W.A., "Reduction of Base Drag by Gas Ejection," Rept. 4×69, Royal Armament Research and Development Establishment, Fort Halstead, Kent, U.K., Dec 1969.
- ⁶Clayden, W.A. and Bowman, J.E., "Cylindrical Afterbodies at $M=\infty$ 2 with Hot Gas Ejection," *AIAA Journal*, Vol. 6, Dec. 1968, pp. 2429-2430.
- ⁷Bowman, J.E. and Clayden, W.A., "Boat-Tailed Afterbodies at $M_\infty=2$ with Gas Ejection," *AIAA Journal*, Vol. 6, Oct. 1968, pp. 2029-2030.
- ⁸Freeman, L.M. and Korkegi, R.H., "Projectile Aft-Body Drag Reduction by Combined Boat-Tailing and Base Blowing," AFAPL-TR-75-112, Air Force Aero Propulsion Laboratory, Wright-Patterson Air Force Base, Ohio, Feb. 1976.
- ⁹Bowman, J.E. and Clayden, W.A., "Cylindrical Afterbodies in Supersonic Flow with Gas Ejection," *AIAA Journal*, Vol. 5, Aug. 1967, pp. 1524-1525.
- ¹⁰Proceedings of the Workshop on Aerodynamics of Base Combustion, School of Mechanical Engineering, Purdue University, sponsored by Interior Ballistics Laboratory, Ballistic Research Laboratories, Aberdeen Proving Ground, Md., May 29-30, 1974.

Wake Effects in Finite Amplitude Nonsteady Motion of Slender Profiles

M.G. Chopra*

University of Cambridge, Cambridge, England

Introduction

NONSTEADY motion of thin wings is always accompanied by shedding of the boundary layer from the separation point in the form of a thin sheet deforming into vortices. It is possible to obtain a reasonably accurate description of this phenomenon from the study of ideal fluid motion, using Kutta condition for determining circulation, provided the medium in which the wing moves has small viscosity, and the angle of incidence is small. Karman and Sears,¹ Kuessner,² and Theodorsen³ developed unsteady aerofoil theory. Their results, based on the additional assumption that the trailing edge of the profile traverses rectilinear path, found extensive applications in aerodynamics as well as ship-hydrodynamics. This theory has significant applications in animal locomotion. Lighthill⁴ studied the lunette-tail hydrodynamics using Prandtl's acceleration potential method which earlier had found brilliant applications in Possio's⁵

Received June 30, 1975; revision received Jan. 27, 1976. The author is grateful to Sir James Lighthill FRS, Lucasian Professor, for providing an opportunity to work with him and for many useful suggestions, and to the Association of Commonwealth Universities for a post-doctoral award.

Index categories: Nonsteady Aerodynamics.

*Presently Senior Scientific Officer, Defence Science Laboratory, Delhi, India.

work on unsteady aerofoil motion in compressible medium and Wu's⁶ work on the swimming efficiency of thin plates. The author⁷ based his analysis of the unsteady motion of the caudal fin on the vorticity distribution, and he found it convenient to incorporate the effect of the streamwise vorticity in the wake which was neglected in Lighthill's two-dimensional study. However, the investigation of the actual finite amplitude motion asks for the generalization of Karman and Sear's¹ results for the nonrectilinear wake. A method is given here for finding the vortex intensity induced on the aerofoil due to an arbitrarily placed wake vortex. This in turn will help in the evaluation of the wake vorticity, and the procedure for determining the complete wing and wake vortex system is outlined.

Effect of Wake Vortices

The effect of an element of wake vorticity Γ' positioned at a point z_i may be evaluated by the method of conformal transformation. The aerofoil is mapped on to a circle in the z' -plane through

$$z + c = z' + a^2/z' \quad (1)$$

where $a = c/2$ (Fig. 1) and the method of images in conjunction with Joukowski's condition of smooth flow past the trailing edge yields

$$\Gamma'' = \Gamma' (z_i' z_i' - a^2) / [(a - z_i') (a - \bar{z}_i')] \quad (2)$$

Total vorticity induced by a point vortex Γ' located at z_i is

$$\Gamma = \Gamma' \left\{ \frac{z_i' \bar{z}_i' - a^2}{(a - z_i') (a - \bar{z}_i')} - 1 \right\} \quad (3)$$

and the vortex intensity induced on the aerofoil, say $\gamma_i(x)$, is given by

$$\gamma_i(x) = \frac{\Gamma'}{2\pi(c^2 - (c+x)^2)^{1/2}} \frac{\alpha_i}{\beta} [2 - \beta\{\delta - (x+c)x_i' - (c^2 - (c+x)^2)^{1/2} y_i'\}^{-1} - \beta\{\delta - (x+c)x_i' + (c^2 - (c+x)^2)^{1/2} y_i'\}^{-1}] \quad (4)$$

where

$$\alpha_i = x_i'^2 + y_i'^2 - a^2, \quad \delta = x_i'^2 + y_i'^2 + a^2, \quad \beta = \delta - 2ax_i'$$

and z_i' is known in terms of z_i through Eq. (1).

For a rectilinear wake Eqs. (3) and (4) reduce to

$$\Gamma = \Gamma' \left\{ \left(\frac{x_i + 2c}{x_i} \right)^{1/2} - 1 \right\}$$

and

$$\gamma_i(x) = \frac{1}{\pi} \frac{\Gamma'}{(x_i - x)} \left(\frac{-x}{x+2c} \right)^{1/2} \left(\frac{x_i + 2c}{x_i} \right)^{1/2}$$

which agree with Eqs. (7) and (8) of Karman and Sears.¹

The vortex intensity induced on the aerofoil by wake vortices lying on a sinusoidal path (with respect to OXY) is plotted in Figs. 2a, b, and c. Figure 2a depicts a behavior similar to that observed by Karman and Sears¹ but with a reduced intensity. For example, the vortices very close to the trailing edge induce very strong vorticity on the aerofoil with a definite peak near the trailing edge in addition to the one at the leading edge, whereas vortices located a little farther off from the trailing edge induce vortex intensity akin to that produced by small angle of incidence. It is interesting to note that as the amplitude of the path increases the wake vortices very close to the trailing edge are able to force back flow giving rise to negative vortex intensity on the rear part of the

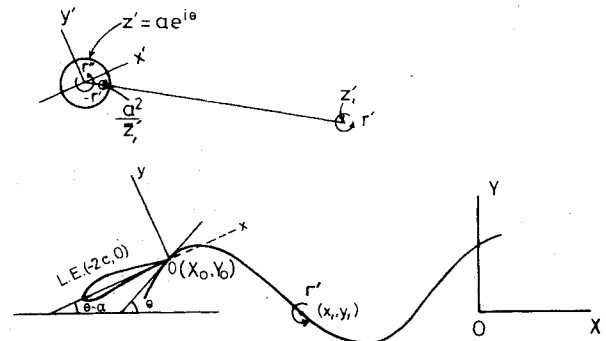


Fig. 1 Diagram showing notation employed, and the conformal representation of the aerofoil and a wake vortex for finite amplitude motion.

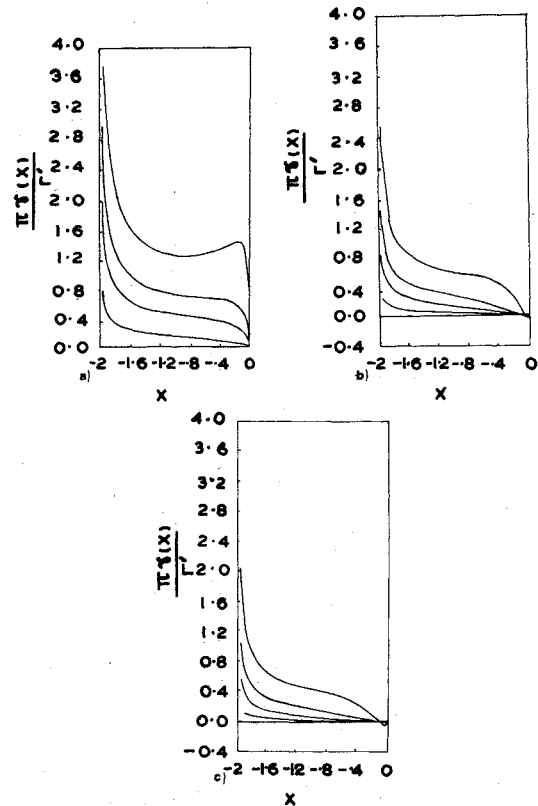


Fig. 2 Diagram showing the plot of vorticity distribution, $(\pi\gamma(x)/\Gamma')$ on the aerofoil from the leading to the trailing edge induced by a wake vortex Γ' positioned at various distances from the trailing edge. The wake vortex is supposed to lie on a sinusoidal curve having wave length $4\pi c$. Curves from top to bottom are for vortices stationed at points having the abscissa $0.1c$, $0.35c$, $0.50c$, and $2.0c$, respectively. The amplitude of the curve is c in Fig. 2a, $5c$ in Fig. 2b and $7c$ in Fig. 2c.

aerofoil. This phenomenon starts getting exhibited in Fig. 2b but becomes more apparent in Fig. 2c. The analysis may also throw some light on the maximum angle of incidence that can be achieved in finite amplitude motion without effecting separation. Figure 3 gives the total induced vorticity scaled on the intensity of the vortex wake for various values of the amplitude and revives the result that the vortices close to the trailing edge induce higher vorticity than those that are farther off.

Determination of Complete Vortex Distribution

Let the path of the trailing edge of the aerofoil referred to a frame of reference fixed in the fluid at rest be $X = X_0(t)$, $Y = Y_0(t)$. The direction of the path $\theta(t)$ will be given

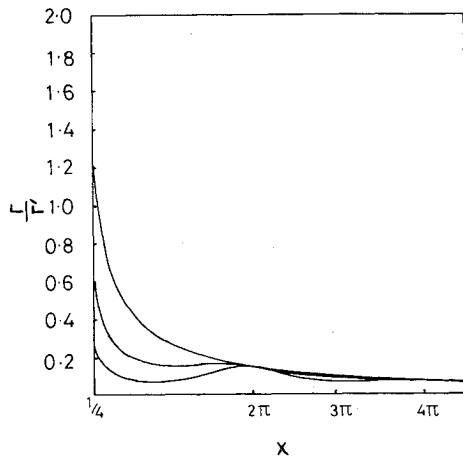


Fig. 3 Diagram showing the plot of the total induced vorticity (Γ/Γ_0) against the abscissa of the position of the wake vortex. The sinusoidal curve has wavelength $4\pi c$, and the curves from top to bottom are for amplitudes 0.0, $1.0c$, and $2.0c$, respectively.

by $\theta(t) = \tan^{-1} \{ \dot{Y}_0(t)/\dot{X}_0(t) \}$ where the dot denotes differentiation with respect to time. At any instant of time, let the angle of attack (assumed small) be $\alpha(t)$, and therefore the aerofoil will be inclined at an angle $\theta(t) - \alpha(t)$ to the x -axis. The transformation from the coordinate system fixed in the aerofoil to the coordinate system fixed in the fluid at rest can be effected through

$$x = (X - X_0) \cos(\theta - \alpha) + (Y - Y_0) \sin(\theta - \alpha) \quad (5a)$$

$$y = (Y - Y_0) \cos(\theta - \alpha) - (X - X_0) \sin(\theta - \alpha) \quad (5b)$$

and the velocity of the aerofoil referred to the xoy system is

$$[\dot{X}_0(t) \sec \theta, -\alpha \dot{X}_0(t) \sec \theta + x(\dot{\theta} - \dot{\alpha})]$$

Assuming that the flow about the aerofoil is two-dimensional, the movement of any part of the aerofoil from the path described by the trailing edge is small, and that the vortices shed from the trailing edge may lie along the path of the trailing edge, the analysis can be carried out without excessive complications.

Munk's^{8,9} theory gives

$$\frac{d\Phi}{dz} \left(\frac{z+2c}{z} \right)^{1/2} = -\frac{1}{i\pi} \int_{-2c}^0 \frac{\alpha \dot{X}_0 \sec \theta - \xi(\dot{\theta} - \dot{\alpha})}{(\xi - z)} \left(\frac{2c + \xi}{-\xi} \right)^{1/2} d\xi \quad (6)$$

where $d\Phi/dz$ is the complex velocity. Using Eq. (6), the clockwise vortex intensity, $\gamma_0(x)$, is given by

$$\gamma_0(x) = -2u(x, 0-) = 2 \left(\frac{-x}{x+2c} \right)^{1/2} \{ -\alpha \dot{X}_0 \sec \theta + (x+c)(\dot{\theta} - \dot{\alpha}) \}$$

Total quasisteady vorticity on the aerofoil, say Γ_0 resulting from its motion, if the wake had no effect, is given by

$$\Gamma_0 = \int_{-2c}^0 \gamma_0(x) dx = -\pi c \{ 2\alpha \dot{X}_0 \sec \theta + c(\dot{\theta} - \dot{\alpha}) \} \quad (7)$$

If the wake vortex intensity is $\gamma(x_l)$, which is still unknown, the total vorticity induced on the aerofoil Γ_l , by the whole wake, using Eq. (4), works out to be

$$\Gamma_l = \int_0^l \gamma(x_l) \left(\frac{\alpha_l}{\beta} - l \right) \left(\left(\frac{dy_l}{dx_l} \right)^2 + l \right)^{1/2} dx_l \quad (8)$$

where dy_l/dx_l is the slope of the path referred to the xoy system, and l is the x -coordinate of the farthest point of the wake. Total vorticity in the wake, Γ_w is

$$\Gamma_w = \int_0^l \gamma(x_l) \left(\left(\frac{dy_l}{dx_l} \right)^2 + l \right)^{1/2} dx_l \quad (9)$$

Conservation of circulation, viz., $\Gamma_0 + \Gamma_l + \Gamma_w = 0$ yields the integral equation

$$\pi c \{ 2\alpha \dot{X}_0 \sec \theta + c(\dot{\theta} - \dot{\alpha}) \}$$

$$= \int_0^l \gamma(x_l) \frac{\alpha_l}{\beta} \left(\left(\frac{dy_l}{dx_l} \right)^2 + l \right)^{1/2} dx_l$$

which referred to fixed coordinate system OXY transforms to

$$\Gamma_0 = \int_{X_0}^{X_l} \gamma(X_l) f(X_l, X_0) \sec \theta_l dX_l$$

where $\theta_l = \tan^{-1} \{ dY_l/dX_l \}$ and $f(X_l, X_0) = \alpha_l/\beta$ can be evaluated for each value of X_l through Eqs. (1) and (5). The kernel $f(X_l, X_0)$ has a square root singularity at the trailing edge, X_0 , and as such the normal procedure of obtaining the integral equation of the second kind by differentiating with respect to the lower limit of integration cannot be adopted as elucidated by Mangler.¹⁰ However, for periodic oscillations, the vorticity shed in the wake is periodic with zero mean and accordingly

$$\Gamma_0 = \int_{X_0}^{X_0+X_p} \gamma(X_l) \left[\sum_{n=1}^{\infty} f(X_l + n - l X_p, X_0) \right] \sec \theta_l dX_l + \Gamma_w \quad (10)$$

where X_p is the period of the oscillation, and Γ_w , accounting for the fluctuations of the wake vorticity¹¹ which vanishes if the wake consists of a finite whole number of periods, is periodic in X_0 with zero mean and is given by

$$d\Gamma_w/dX_0 = -\gamma(X_0) \sec \theta \quad (11)$$

The convergence of the kernel in Eq. (10) can be achieved by subtracting a suitable constant (varying appropriately with the number of periods taken into account). The square root singularity can be taken care of by a simple transformation of the variable of integration through

$$X_l = X_0 + u^2$$

These modifications render Eq. (10) in a form amenable to solution by standard procedures. Thus the wake vorticity is known which in turn through Eq. (4) gives the vortex intensity induced on the aerofoil. Thus the complete vorticity distribution is known, and the analysis can be followed up for the evaluation of lift, moment, and drag for the problems of aerodynamic and ship-hydrodynamic interest, or for the calculation of the forward thrust and subsequently hydromechanical propulsive efficiency for the problems of animal locomotion on the lines of Karman and Sears¹ and Chopra,^{7,11} respectively.

In conclusion, the vortex intensity and vorticity induced on an aerofoil by an arbitrarily stationed wake vortex has been calculated, and a method for the evaluation of the complete vorticity distribution for the case of an aerofoil making finite amplitude oscillations is outlined.

References

- 1 Karman, T. and Sears, W.R., "Aerofoil Theory for Non-Uniform Motion," *Journal of Aeronautical Sciences*, Vol. 5, Aug. 1938, pp. 379-390.

²Kuessner, H.G., "General Aerofoil Theory," *Luftfahrt Forschung*, Vol. 17, 1940, pp. 370-378.

³Theodorsen, T., "General Theory of Aerodynamic Instability and the Mechanism of Flutter," NACA Rept. 496, Washington, D.C., 1935.

⁴Lighthill, M.J., "Aquatic Animal Propulsion of High Hydro-Mechanical Efficiency," *Journal of Fluid Mechanics*, Vol. 44, Pt. 2, 1970, pp. 265-301.

⁵Possio, C., "The Problem of Unsteady Motion of a Wing," *Aerotecnica*, Vol. 20, 1940, pp. 655-681.

⁶Wu, T.Y., "Swimming of Waving Plate," *Journal of Fluid Mechanics*, Vol. 10, Pt. 3, 1961, pp. 321-344.

⁷Chopra, M.G., "Hydromechanics of Lunate-Tail Swimming Propulsion," *Journal of Fluid Mechanics*, Vol. 64, Pt. 2, 1974, pp. 375-391.

⁸Munk, M.M., "General Theory of Thin Wing Sections, NACA Rept. 142, 1922.

⁹Munk, M.M., "Elements of the Wing Section Theory and of the Wing Theory," NACA Rept. 192, 1924.

¹⁰Mangler, K., "Improper Integrals in Aerodynamics," Royal Aircraft Establishment, Farnborough, U.K., Rept. Aero 2424.

¹¹Chopra, M.G., "Large-Amplitude Lunate Tail Theory of Fish Locomotion," *Journal of Fluid Mechanics*, Vol. 74, March 1976, pp. 161-182.

Influence of Nonconservative Differencing on Transonic Streamline Shapes

Perry A. Newman* and Jerry C. South Jr.†
NASA Langley Research Center, Hampton, Va.

THE basic relaxation technique introduced by Murman and Cole¹ has been used extensively in computing transonic flowfields. A deficiency was later recognized in the original finite-difference scheme and Murman² introduced a conservative finite-difference scheme, which included a shock-point operator, in order to correct it. Nevertheless, the original nonconservative scheme continues to be used by most investigators since it seems to give shock jumps and locations at the surface of the configuration more nearly like those observed in experiments. The purpose of this Note is to demonstrate that these nonconservative shocks, which may extend well into the flowfield, destroy the global mass balance by producing mass at the shock. In a transonic internal (or confined) flow this lack of mass balance may prove to be more crucial than is the case for an unconfined external flow.

The present results and observations were prompted by streamtube anomalies first noted in calculations pertaining to wind tunnel flows in both 2 and 3 dimensions. The influence of conservative vs nonconservative finite-difference formulation on the global mass balance is readily observed by computing streamline shapes in an external 2-D transonic flow. This Note presents such samples; some additional detail and material was given limited distribution in Ref. 3.

Problem Description

A NASA Langley study of one concept for minimizing wind-tunnel interference involves contouring the upper and lower (initially solid) walls of a small 2-D facility according to numerical results obtained from nonlinear flow solutions. Calculated free-air streamline deflections at the proposed tunnel-wall locations for subsonic lifting flow showed that a streamtube, roughly the dimensions of the tunnel, returned to

Received April 15, 1976.

Index category: Subsonic and Transonic Flow.

*Aero-Space Technologist, Theoretical Aerodynamics Branch, Subsonic-Transonic Aerodynamics Division.

†Assistant Head, Theoretical Aerodynamics Branch, Subsonic-Transonic Aerodynamics Division. Associate Fellow AIAA.

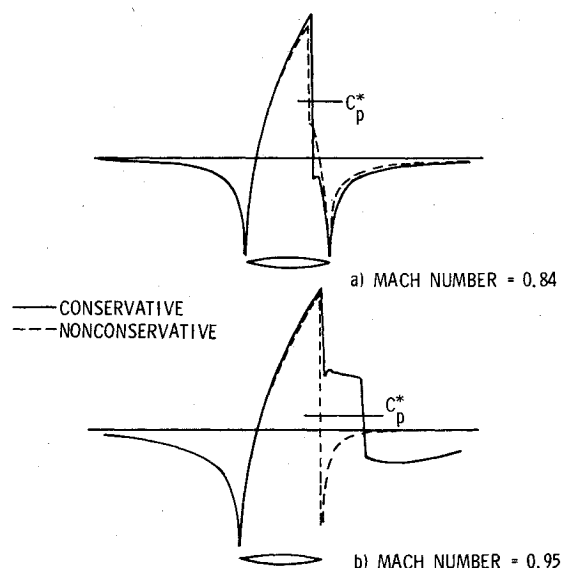


Fig. 1 Computed pressure coefficients along symmetry line for nonlifting transonic flow past 10% thick parabolic arc airfoil.

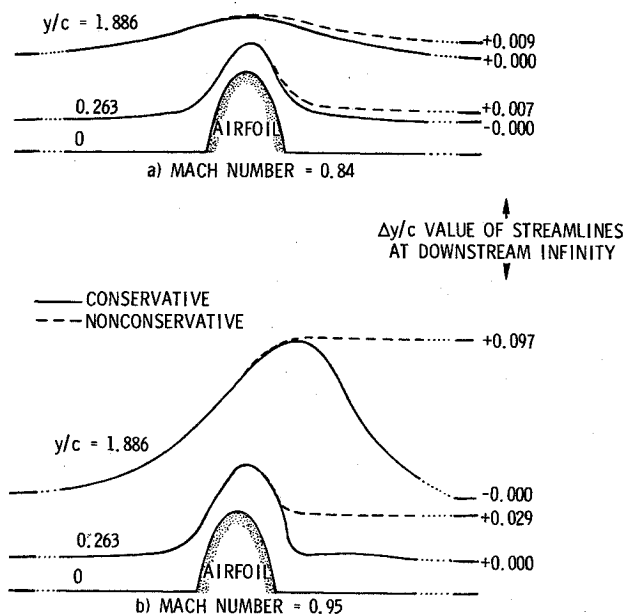


Fig. 2 Computed streamline deflections for nonlifting transonic flow past 10% thick parabolic arc airfoil.

its far-upstream size far downstream of the model. That is, there was a global mass balance in the calculation. Similar calculations for supercritical lifting flow with shocks, however, showed that the size of the streamtube had increased from far upstream to far downstream, indicating that mass had been introduced. These results were generated using a program which employed the Garabedian and Korn⁴ non-conservative finite-difference scheme.

A computer program recently developed by South and Brandt⁵ contained the Murman² conservative finite-difference scheme and was easily modified to use the Garabedian and Korn⁴ nonconservative finite-difference scheme. This program solves the transonic small disturbance equation for only symmetric flow, but incorporates several iterative solution techniques. For the results presented here, the equally-spaced computational grid was analytically stretched so that the physical grid extended to infinity in both the streamwise and normal directions. Streamline shapes were obtained along several grid lines by a streamwise integration of the normal component of the perturbation velocity.